COMMUNICATION

Dynamic, 3D-Pattern Formation Within Enzyme-Responsive Hydrogels

By *Karin S. Straley* and *Sarah C. Heilshorn**

Recent advancements in biology and medicine have placed significant emphasis on the development of fabrication strategies that generate three-dimensional (3D) biochemical, mechanical, and spatial patterns within soft, biocompatible hydrogels.[1–4] Patterned hydrogels are often designed to mimic natural tissue and are mainly used in tissue engineering studies (e.g., liver, kidney, neuronal, and vascular applications) and fundamental studies of cellular response to chemical or physical cues.[5–8] Current technologies for patterning hydrogels have focused on creating features using layer-by-layer stacking (fused with heat, adhesives, or light),[2] molding,[9,10] 3D printing,[11] electrochemical deposition,[12] and photolithography.[5,13] These technologies have proven to be successful in producing intricate patterns within hydrogels but only address applications that require static features present before material implantation or experimentation.

In this work we propose a new method to create dynamic, 3D hydrogel patterns involving layered spatial deposition of chemically crosslinked, biodegradable polymers. By arranging polymers with widely different and controlled degradation rates within a single composite hydrogel material, patterns can be enzymatically triggered to emerge over time in response to biologically relevant proteases. These patterns can be created in the form of either completely internal voids contained within well-sealed structures or as open-geometry configurations, since the composite hydrogel microstructure supports rapid diffusion of both proteases and material degradation fragments. In addition, the material released during the formation of either pattern type can be modified to serve as a drug-delivery vehicle. Here, we demonstrate the synthesis and characterization of polymers with highly tunable degradation rates, the evolution of 3D internal and open structures within composite polymeric materials, and the use of spatial and temporal patterns to deliver fluorochromic molecules with distinct delivery profiles.

While our approach can be applied to other types of biodegradable polymer, we have chosen to use recombinant, engineered protein polymers that contain peptide regions susceptible to cleavage by cell-secreted proteases at predictable and tunable rates. Protein-based materials often offer inherent biocompatibility, can be degraded into non-cytotoxic fragments, and possess similar properties to native tissue, greatly facilitating their use as engineered cell scaffolds.[14,15] Furthermore, protein polymers are synthesized using genetic templates, which allow for precise molecular-level control over the polymer content and, therefore, over the degradation rate. The specific amino acid compositions of our engineered proteins are detailed in Figure 1a. Evident in this figure is their repetitive and modular design, consisting of alternating active and structural domains.[16,17] The structural domains are based upon a well-known sequence borrowed from the protein elastin that imparts properties of mechanical resilience and elasticity.[18,19] The intermittent active domains contain short amino acid sequences, previously selected through analysis of a four-amino acid peptide library,[20] that exhibit varying susceptibility to cleavage by the enzymes, tissue plasminogen activator (tPA), and urokinase plasminogen activator (uPA). These enzymes are members of the serine-protease family, are primarily produced in vivo by endothelial and neuronal cells, and have been linked to physiological roles in thrombolysis (blood-clot dissolution) and extracellular-matrix (ECM) degradation. For each enzyme, sequences were chosen to generate predicted fast-degrading (t1, u1), medium-degrading (t2, u2), and slow-degrading (t3, u3) protein polymers. An additional active domain, with a predicted limited vulnerability to both tPA and uPA cleavage, containing the well-known integrin-binding RGD sequence from the natural ECM protein fibronectin was also selected for synthesis.[21] This same protein polymer was previously described to control adhesion and neurite elongation of neuronal-like PC-12 cell cultures.[22] Unlike hydrogel scaffolds that utilize crosslinking peptides as targets for enzymatic biodegradation, these protein-polymer scaffolds enable independent tuning of the initial mechanical properties and the subsequent biodegradation kinetics.[22–25]

Prior to characterization, all protein polymers were expressed in *Escherichia coli* bacteria and purified. Comparative degradation rates were first evaluated for protein polymers solubilized in buffer and exposed to high concentrations of either tPA or uPA enzyme. The experimental degradation rate trends were found to match the predictions from the four-amino acid peptide library for all proteins except t1 (Fig. 1b, Supporting Information Fig. S1 and S2). By changing only 3% of the protein–amino acid composition, the half-lives of the uPA cleavable proteins were tuned across a 200-fold range and the tPA-cleavable proteins were tuned across a 10-fold range. This high level of tunability greatly supports the use of short peptide domains as tunable targets for

[*] Prof. S. C. Heilshorn
Materials Science and Engineering Department
Stanford University
476 Lomita Mall, McCullough Building 246
Stanford, CA 94305–4045 (USA)
E-mail: heilshorn@stanford.edu
Dr. K. S. Straley
Chemical Engineering Department
Stanford University
476 Lomita Mall, McCullough Building 246
Stanford, CA 94305–4045 (USA)

DOI: 10.1002/adma.200901865

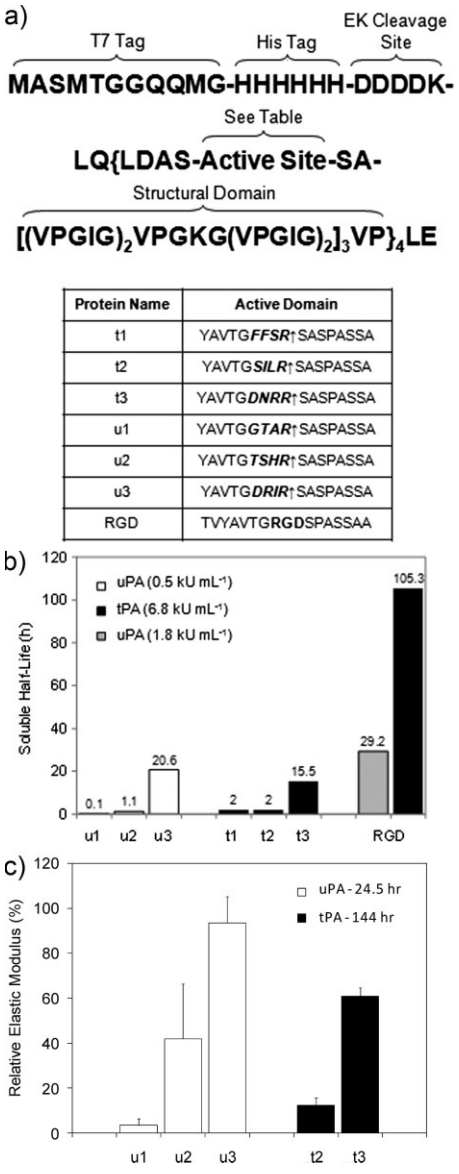

Protein Name	Active Domain
t1	YAVTG***FFSR***↑SASPASSA
t2	YAVTG***SILR***↑SASPASSA
t3	YAVTG***DNRR***↑SASPASSA
u1	YAVTG***GTAR***↑SASPASSA
u2	YAVTG***TSHR***↑SASPASSA
u3	YAVTG***DRIR***↑SASPASSA
RGD	TVYAVTG**RGD**SPASSAA

Figure 1. Design of engineered proteins with tunable degradation rates. a) Amino acid sequences of the full-length recombinant proteins and their specific active domains shown as single-letter amino acid abbreviations (EK refers to enterokinase, ↑ refers to the predicted protease cut site, four-amino acid peptide sequences previously screened for degradation rate shown in italics). b) Comparison of soluble-protein half-lives after cleavage at high enzyme concentrations (uPA = 0.5 kU mL^{-1} for all uPA cleavable proteins, 1.8 kU mL^{-1} for RGD; tPA = 6.8 kU mL^{-1} for all tPA cleavable proteins and RGD). c) Comparison of relative changes in the compressive elastic modulus of crosslinked hydrogels after cleavage at high enzyme concentrations (uPA = 0.3 kU mL^{-1}; tPA = 6.8 kU mL^{-1}).

tPA- and uPA-induced cleavage in biodegradable materials. Since t1 and t2 degraded at similar rates and t2 expressed at much higher levels, t1 was not further analyzed. Also, as predicted, the RGD polymer degraded very slowly in response to both tPA and uPA, thus solidifying its use as a more permanent, cell-adhesive polymer. By submitting several degradation fragments of these reactions for N-terminal protein sequencing, a high degree of degradation specificity was confirmed; the prominent final degradation bands present on electrophoretic gels corresponded to the molecular weight of the smallest designed cleavage fragment (Fig. S1). A direct comparison between all predicted and actual protein degradation fragment sizes also supported high degradation-reaction specificity.[22]

Next, the engineered proteins were crosslinked into gels using a bifunctional amine-reactive chemical crosslinker, disuccinimidyl suberate (DSS), which reacts with free amine groups presented by lysine residues (single letter abbreviation: K) within the protein structural domains (Fig. 1a). Despite the initial solubilization of DSS in an organic solvent, previous work measuring the proliferative capacity of cells grown in 2D cultures on the surface of thoroughly washed DSS crosslinked protein films showed no evidence of cytotoxicity (Fig. S3).[22] For applications requiring 3D cell culture, an alternative crosslinking strategy, using the trifunctional amine-reactive chemical crosslinker β-[tris(hydroxymethyl) phosphino] propionic acid (THPP), is used to eliminate the need for organic solvents and to allow cells to be fully encapsulated within the hydrogel structure.[26] The cell compatibility of this crosslinking method is demonstrated by the encapsulation and subsequent differentiation and neurite extension of neuronal-like PC-12 cells within our hydrogels (Fig. S4).

The degradation properties of the crosslinked hydrogels were characterized upon exposure to high concentrations of tPA or uPA enzymes by monitoring changes in the elastic modulus over time (Fig. 1c). To simplify data comparison, all elastic moduli were normalized to the initial time-zero elastic modulus value of each sample (the average initial elastic modulus was 44 ± 11 kPa, Table S1). As expected, the degradation rate trends exhibited by the soluble polymers translate into tunable degradation of the crosslinked hydrogels. The uPA-degradable materials show a 28-fold difference in elastic modulus change over a 24-hour time period, and the tPA-degradable materials show a 5-fold difference in elastic modulus change over a 144-hour time period.

These polymers with highly tunable degradation rates are ideal substrates to create dynamic, 3D hydrogel patterns. By spatially patterning polymers with differing degradation rates inside a single composite material, patterns are induced to emerge over time in the presence of enzymes. To form 3D composites, the individual layers were first crosslinked separately into specific shapes and then covalently fused together in a subsequent crosslinking step. This procedure can be repeated as necessary to generate a variety of 3D patterns. As initial proof of concept, a single, long channel was designed to emerge over time within a u3 hydrogel due to sacrificial degradation of a u1 region (Fig. 2a,b). Distinct layers are visible in the images of the composite hydrogel due to its sequential formation during multiple crosslinking steps (Fig. 2b–d). Initially, the composite hydrogel was a continuous slab of polymer; however, upon exposure to the uPA enzyme, the u1 region quickly degraded away within 3 days to reveal a long, open channel running the entire length of the hydrogel. The remaining u3 polymer retained enough structural integrity to maintain this open channel with a predetermined geometry of $\sim$1 mm $\times$ 3 mm $\times$ 2 mm, H $\times$ W $\times$ L (Fig. 2c,d).

To develop dynamic patterns that emerge to form a completely internal architecture within a well-sealed outer hydrogel, we

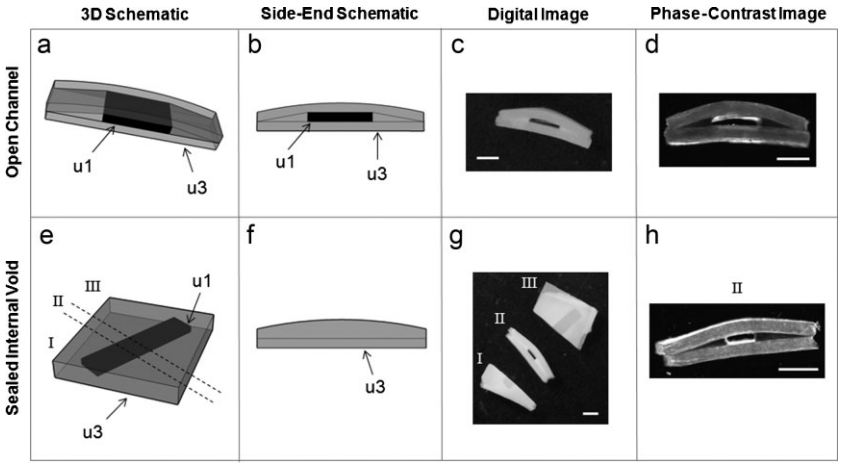

Figure 2. Emergence of both an open channel and a completely sealed internal void within composite hydrogel structures during treatment with 0.3 kU mL^{-1} uPA. a–d) Evolution of open channel through the hydrogel: a) schematic of the 3D multilayer structure, b) schematic depicting a side-end view of the patterned hydrogel, c) digital photograph of hydrogel at $t = 3$ days, showing that the open channel has emerged along the entire length of the hydrogel; d) phase-contrast image at $t = 3$ days. e–g) Evolution of an entirely internal void within a well-sealed hydrogel: e) schematic of the 3D multilayer structure (dashed lines indicate cut site for visualization of internal structure), f) schematic depicting a side-end view of the patterned hydrogel, g) digital photograph of hydrogel at $t = 3$ days showing the emergence of an internal structure (center piece (II) cut from full structure and flipped on edge), h) phase-contrast image of center piece (II, on edge) at $t = 3$ days; scale bar = 2 mm.

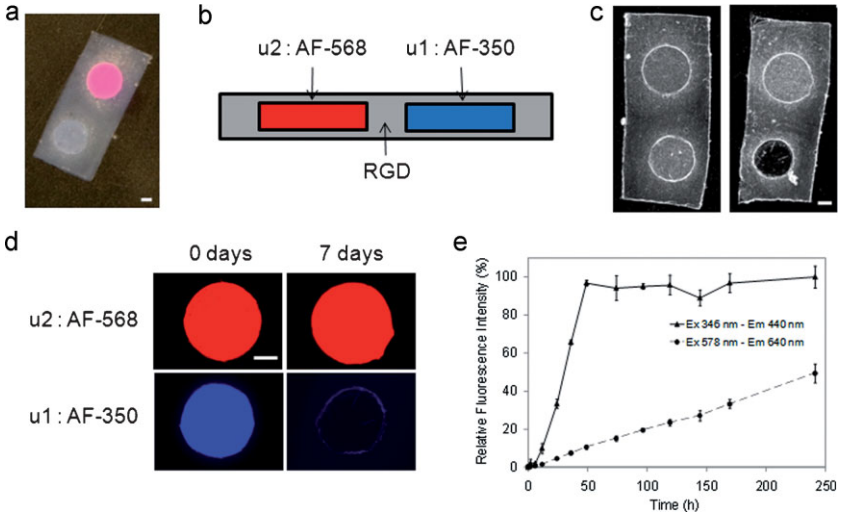

Figure 3. Controlled spatial and temporal delivery of fluorescent molecules in conjunction with hydrogel pattern evolution. a) Digital image of fluorescently labeled, patterned hydrogel (top circle = u2:AF-568, bottom circle = u1:AF-350, surrounding scaffold = RGD). b) Schematic depicting a longitudinal cross-section of the patterned hydrogel showing placement of the internal fluorophore reservoirs within the sealed RGD hydrogel. c) Phase-contrast image of samples before (left) and after (right) degradation with 0.3 kU mL^{-1} uPA. d) Fluorescent images of labeled u1 and u2 regions at $t = 0$ and 7 days. e) Time course of solution fluorescence intensity, AF:568 Ex–Em = 578–640 nm and AF:350 Ex–Em = 346–440 nm; scale bar = 1 mm.

carefully examined the potential diffusion limitations presented by the hydrogel microstructure.[27] The successful formation of these internal patterns requires a proper balance between the designed molecular weight of the polymer degradation fragments, the protease hydrodynamic diameter, and the crosslinked hydrogel structure. As a demonstration, an internal sacrificial column of u1 was completely encased within a sealed u3 scaffold (Fig. 2e,f). Previous work has shown that our hydrogels contain approximately 85% water when swollen, thus facilitating the diffusion of relatively small enzymes (uPA ~33–54 kDa, tPA ~59 kDa) and the designed polymer degradation fragments (~4–8.7 kDa) throughout the scaffold.[22] By changing the frequency and location of the protease-cleavable active domains within the protein primary sequence, the sizes of the predicted polymer degradation fragments and their relative diffusion rates can be precisely controlled. Effective enzyme and polymer fragment diffusion within our scaffold structure was confirmed when the second composite hydrogel was exposed to uPA, resulting in the emergence of a predesigned internal void within the well-sealed outer hydrogel (Fig. 2g,h). The minimum diffusion path in this geometry was ~1 mm wide, which required diffusion across a length similar in magnitude to the currently recognized nutrient diffusion limit of 2 mm in natural tissue.[28,29] While current hydrogel patterning techniques aim to mimic static features of complex ECM tissue, this new dynamic approach allows hydrogels to adapt and develop over time as 3D patterns emerge within the material. This technique has the potential to offer an added layer of complex control, in which the formation of patterns can be directly tied to cellular growth and cell-secreted proteases.

The time-dependent, enzyme-induced evolution of patterns within hydrogels can also be used to release multiple tethered molecules, each with a distinct spatial and temporal delivery profile. To demonstrate this application, two different fluorescent molecules, AlexaFluor(AF)-350 and AF-568, were covalently linked to two proteins with different degradation properties, u1 and u2. These labeled materials were spatially patterned as internal reservoirs within a sealed, cell-adhesive, non-degrading RGD hydrogel to form a single composite structure (Fig. 3a,b). Upon exposure to uPA, the specific release of the tethered molecules was confirmed using both phase and fluorescence microscopy (Fig. 3c,d). In addition, the time-dependent release of each fluorescent molecule was monitored with fluorescence spectroscopy; the data collected for each fluorescent molecule were normalized to the fluorescence value of a solution containing the fully released molecule of interest (Fig. 3e). A complete, burstlike delivery profile was observed for u1-tethered AF-350, while a sustained delivery profile was seen for u2-tethered AF-568 (Fig. 3e). Several examples in the literature have demonstrated

that drugs or proteins that are covalently linked to scaffolds, using mechanisms similar to our AF-350 and AF-568 linkage reaction, can retain their biological activity.[30,31] Together our results demonstrate the potential for using adaptive hydrogels to deliver multiple drugs with highly distinct temporal and spatial delivery profiles and the ability to couple drug release to cell behavior within a growth-promoting environment.

The successful application and integration of our adaptive hydrogels into medical therapies will ultimately require extensive and precise tuning of material degradation and molecular delivery rates to effectively meet tissue-specific, in vivo requirements. For example, in peripheral nerve regeneration applications, it has been hypothesized that hydrogel implants must be degradable to avoid physical inhibition of nerve growth and that the optimal degradation half-life of these implants should match the rate of nerve regeneration, approximately 2–4 weeks.[32–35] In an effort to mimic potential physiological conditions present in such neuronal applications, biologically relevant tPA and uPA concentrations were approximated by performing an enzyme-linked immunosorbent assay (ELISA) on PC-12 neuronal-like culture supernatants. These decreased enzyme conditions resulted in the predictable extension of scaffold degradation rate trends over a one-month period and place our hydrogels within the proposed optimal degradation rate range for neuronal materials (Fig. S5). Furthermore, the degradation rate of the hydrogels can be fine-tuned by uniformly mixing together proteins with variable degradation susceptibility within a single hydrogel, thus creating scaffolds that exhibit intermediate degradation rates (Fig. S6). As a result, we predict that a full range of scaffolds can be created with identical initial elastic moduli and exquisitely tunable degradation rates.

The optimization of our initial scaffold modulus impacts our choice of scaffold degradation rate and can be further applied to meet the demands of individual tissues, since cells have been extensively shown to respond to mechanical properties.[36–38] The initial elastic modulus of the entire composite material or of specific patterned regions within the hydrogel can be controlled by simply varying the amount of chemical crosslinker used during fabrication (Fig. S7). Future optimization studies of our scaffolds will focus on material degradation by multiple proteases because tPA and uPA may be simultaneously present at injury sites. Initial crossreactivity characterization studies have been conducted showing some evidence of tPA-degradation susceptibility by the designed uPA-cleavage proteins and vice versa (Fig. S1 and S2). The ability to tune scaffold degradation as a function of multiple cell-secreted enzymes may lead to applications involving targeted cell infiltration by more than one cell phenotype within distinct regions of the scaffold. Through variation of the active domain content, different enzymes and cell receptors can be targeted with the material, allowing scaffold optimization for specific tissues and cell types.[23]

Overall, our results demonstrate the design of a family of adaptive protein polymers with highly tunable and predictable degradation rates. These protein polymers can be fabricated into hydrogel scaffolds that enzymatically evolve to reveal dynamic, 3D hydrogel patterns. Such patterns can be created in the form of either open geometries or internal voids within well-sealed composite materials due to diffusion of proteases and polymer degradation fragments within the hydrogel microstructure. The inherent functionality of these patterns may be further enhanced through covalent grafting of molecules to the scaffold backbone for controlled spatial and temporal release during pattern evolution. By constructing these scaffolds from recombinant proteins, which offer intrinsic flexibility and precision in polymer content, a wide range of degradation rates and drug-delivery profiles are attainable. With this material we aim to address complex tissue-engineering applications in need of materials that can both adapt to and stimulate cell behavior post-implantation. For example, cell-induced pattern formation can potentially serve as a guidance mechanism for cell migration or as a means to spatially organize cellular co-cultures. Of specific interest may be tissue-regeneration applications that involve multistep cellular development in which optimal scaffold conditions may change over time, such as nerve repair, blood-vessel growth, and stem-cell transplantation. Ultimately, the ability to fabricate enzyme-responsive, 3D-patterned scaffolds opens up possibilities for the future development of engineered constructs that both direct and dynamically evolve with cells.

Experimental

Polymer Synthesis: All protein sequences were cloned into pET15b (Novagen) plasmids using traditional recombinant techniques and expressed in Escherichia coli, BL21(DE3) (induced with 1 mM β-isopropyl thiogalactoside at $OD_{600} \sim 0.6$, 37 °C, expressed for 3–5 h). Proteins were purified using either a previously described inverse temperature-cycling process [22] or nickel-affinity columns (Qiagen). Typical protein yields are ~25–50 mg L^{-1}.

Polymer Crosslinking: Crosslinked hydrogels were prepared by dissolving lyophilized protein (0.1 mg μL^{-1}) in phosphate buffered saline (PBS, pH = 7.4) and rapidly mixing with disuccinimidyl suberate (DSS, Pierce Biotechnology) solubilized in 25:75 dimethyl formamide: dimethyl sulfoxide (DMF:DMSO) solution (0.042 mg DSS μL^{-1} of solvent) at 4 °C. The mixed solution was compressed between two glass plates covered with parafilm (separated with 1-mm spacers) and allowed to react at room temperature (RT, 24 h).

Soluble-Protein Degradation: The soluble-protein degradation reactions were carried out in triplicate at 37 °C (200 µL reaction volume) with either human recombinant tPA (ProspecTany, 6.8 kU mL^{-1}) or low-molecular-weight uPA (Calbiochem, 0.5 kU mL^{-1}) and protein (100 µM) in sodium borate buffer (pH = 8). Samples (6 µL, number of replicates $n = 3$) were taken at specific time points and immediately frozen on dry ice in a solution containing water (9 µL) and 3 × sodium dodecyl sulfate sample buffer (7.5 µL). The extent of degradation was monitored by separating each sample by sodium dodecyl sulfate polyacrylamide gel electrophoresis (12% SDS-PAGE, $n = 3$), staining the degradation fragments with Coomassie Brilliant Blue, and performing densitometry analysis (NIH ImageJ software).

Crosslinked-Protein Degradation: Crosslinked hydrogels were made as described above with a 1:1 stoichiometric ratio of N-hydroxysuccinimide (NHS) esters to primary amines. Crosslinked hydrogels were cut into 3–5-mm-diameter circles. The samples were degraded ($n = 3$) in PBS buffer (pH = 7.4) at RT under constant agitation with either human recombinant tPA (ProspecTany, 6.8 kU mL^{-1}) or mixed high- and low-molecular-weight uPA (Calbiochem, 0.3 kU mL^{-1}). The elastic modulus of each protein was determined ($n = 3$) at the specified time points using a TA AR2000 Rheometer and a compression rate of 2 µm s^{-1}, RT, in PBS buffer (pH = 7.4). Elastic moduli were determined by measuring the slope of the initial linear portion of the stress–strain curve (0–15% strain).

3D Patterning: The individual layers for each structure were prepared separately (u1 and u3) using the same process and conditions as described above (1:1 NHS:primary amines). After ~24 h the crosslinked films were removed from the molds and cut into the desired geometries. These pieces

were then coated in fresh u3 crosslinking solution at 4 °C, organized to achieve the desired spatial pattern, and then allowed to react at RT for another 24 h (within a hydration chamber). The structures were placed in PBS buffer (pH = 7.4) and degraded with mixed high- and low-molecular-weight uPA (Calbiochem, 0.3 kU mL^{-1}) under constant agitation at RT for 3 days. Samples were imaged before and after degradation under phase contrast with a Zeiss Axiovert 200 microscope (2.5 × objective).

Fluorescent-Molecule Delivery: Fluorescently labeled, crosslinked hydrogels were made by dissolving lyophilized u1 or u2 protein (0.1 mg μL^{-1}) in PBS buffer (pH = 7.4, 4 °C) and rapidly mixing with DSS in 25:75 DMF:DMSO solution (0.042 mg DSS μL^{-1} of solvent, 1:1 NHS esters to primary amines) and AF-350 or AF-568 carboxylic acid succinimidyl ester, respectively (Invitrogen, dissolved in 25:75 DMF:DMSO, 0.02:1 molar ratio of carboxylic acid succinimdyl ester to DSS). The remainder of the crosslinking process was the same as described above. The fluorescently labeled, crosslinked films were cut into 3-mm-diameter circles and then embedded within a RGD crosslinking solution that was prepared and crosslinked as described above. RGD gels ($n = 3$) containing one u1:AF-350 circle and one u2:AF-568 circle were placed in PBS buffer (1.1 mL, pH = 7.4) and degraded with mixed high- and low-molecular-weight uPA (Calbiochem, 0.3 kU mL^{-1}) under constant agitation for 9 days at RT. Samples (50 μL, $n = 3$) were taken at the times indicated and analyzed with a Molecular Devices SpectraMax Plus^{384} Spectrophotometer at both 346–440 nm and 578–640 nm (Excitation–Emission (Ex–Em)). A sample of u2:AF-568 was degraded in PBS containing mixed high- and low-molecular-weight uPA (Calbiochem, 2.1 kU mL^{-1}) for 5 days at RT as a reference for fully degraded u2. Samples were imaged before and after degradation under phase contrast and fluorescence with a Zeiss Axiovert 200 microscope (2.5× objective).

Acknowledgements

The authors acknowledge funding support from the National Academies Keck Futures Initiative, the John and Ulla deLarios Scholar Fund, and the Hellman Faculty Scholar Fund. We thank the Stanford Center on Polymer Interfaces and Macromolecular Assemblies for the use of equipment. Supporting Information is available online from Wiley InterScience or from the author.

Received: June 3, 2009
Published online: August 3, 2009

[1] M. S. Hahn, J. S. Miller, J. L. West, *Adv. Mater.* **2006**, *18*, 2679.
[2] V. L. Tsang, S. N. Bhatia, *Adv. Drug Delivery Rev.* **2004**, *56*, 1635.
[3] R. W. Sands, D. J. Mooney, *Curr. Opin. Biotechnol.* **2007**, *18*, 448.
[4] Y. Luo, M. S. Shoichet, *Nat. Mater.* **2004**, *3*, 249.
[5] V. A. Liu, S. N. Bhatia, *Biomed. Microdevices* **2002**, *4*, 257.
[6] J. T. Borenstein, E. J. Weinberg, B. K. Orrick, C. Sundback, M. R. Kaazempur Mofrad, J. P. Vacanti, *Tissue Eng.* **2007**, *13*, 1837.
[7] L. M. Y. Yu, N. D. Leipzig, M. S. Shoichet, *Mater. Today* **2008**, *11*, 36.
[8] J. J. Moon, J. L. West, *Curr. Top. Med. Chem.* **2008**, *8*, 300.
[9] E. Sachlos, N. Reis, C. Ainsley, B. Derby, J. T. Czernuszka, *Biomaterials* **2003**, *24*, 1487.
[10] T. M. G. Chu, S. J. Hollister, J. W. Halloran, S. E. Feinberg, D. G. Orton, *Ann. NY Acad. Sci.* **2002**, *961*, 114.
[11] V. Mironov, T. Boland, T. Trusk, G. Forgacs, R. R. Markwald, *Trends Biotechnol.* **2003**, *21*, 157.
[12] R. Fernandes, L. Q. Wu, T. H. Chen, H. M. Yi, G. W. Rubloff, R. Ghodssi, W. E. Bentley, G. F. Payne, *Langmuir* **2003**, *19*, 4058.
[13] S. H. Lee, J. J. Moon, J. L. West, *Biomaterials* **2008**, *29*, 2962.
[14] S. A. Maskarinec, D. A. Tirrell, *Curr. Opin. Biotechnol.* **2005**, *16*, 422.
[15] R. Langer, D. A. Tirrell, *Nature* **2004**, *428*, 487.
[16] S. C. Heilshorn, J. C. Liu, D. A. Tirrell, *Biomacromolecules* **2005**, *6*, 318.
[17] S. C. Heilshorn, K. A. DiZio, E. R. Welsh, D. A. Tirrell, *Biomaterials* **2003**, *24*, 4245.
[18] A. Nicol, D. C. Gowda, D. W. Urry, *J. Biomed. Mater. Res.* **1992**, *26*, 393.
[19] D. W. Urry, T. M. Parker, M. C. Reid, D. C. Gowda, *J. Bioact. Compat. Polym.* **1991**, *6*, 263.
[20] J. L. Harris, B. J. Backes, F. Leonetti, S. Mahrus, J. A. Ellman, C. S. Craik, *Proc. Nat. Acad. Sci. USA* **2000**, *97*, 7754.
[21] S. Meiners, M. L. T. Mercado, *Mol. Neurobiol.* **2003**, *27*, 177.
[22] K. Straley, S. C. Heilshorn, *Soft Matter* **2009**, *5*, 114.
[23] J. L. West, J. A. Hubbell, *Macromolecules* **1999**, *32*, 241.
[24] S. G. Levesque, M. S. Shoichet, *Bioconjugate Chem.* **2007**, *18*, 874.
[25] S. Kim, E. H. Chung, M. Gilbert, K. E. Healy, *J. Biomed. Mater. Res.* **2005**, *75A*, 73.
[26] D. W. Lim, D. L. Nettles, L. A. Setton, A. Chilkoti, *Biomacromolecules* **2007**, *8*, 1463.
[27] J. L. Drury, D. J. Mooney, *Biomaterials* **2003**, *24*, 4337.
[28] B. R. Zetter, *Ann. Rev. Med.* **1998**, *49*, 407.
[29] C. K. Griffith, C. Miller, R. C. A. Sainson, J. W. Calvert, N. L. Jeon, C. C. W. Hughes, S. C. George, *Tissue Eng.* **2005**, *11*, 257.
[30] S. A. DeLong, J. J. Moon, J. L. West, *Biomaterials* **2005**, *26*, 3227.
[31] M. Ehrbar, V. G. Djonov, C. Schnell, S. A. Tschanz, G. Martiny-Baron, U. Schenk, J. Wood, P. H. Burri, J. A. Hubbell, A. H. Zisch, *Circ. Res.* **2004**, *94*, 1124.
[32] P. J. Apel, J. P. Garrett, P. Sierpinski, J. J. Ma, A. Atala, T. L. Smith, A. Koman, M. E. Van Dyke, *J. Hand Surg. AM* **2008**, *33A*, 1541.
[33] B. A. Harley, M. H. Spilker, J. W. Wu, K. Asano, H. P. Hsu, M. Spector, I. V. Yannas, *Cells Tissues Organs* **2004**, *176*, 153.
[34] R. O. Labrador, M. Buti, X. Navarro, *Exp. Neurol.* **1998**, *149*, 243.
[35] L. R. Williams, F. M. Longo, H. C. Powell, G. Lundborg, S. Varon, *J. Comp. Neurol.* **1983**, *218*, 460.
[36] I. Levental, P. C. Georges, P. A. Janmey, *Soft Matter* **2007**, *3*, 299.
[37] K. Saha, A. J. Keung, E. F. Irwin, Y. Li, L. Little, D. V. Schaffer, K. E. Healy, *Biophys. J.* **2008**, *95*, 4426.
[38] J. B. Leach, X. Q. Brown, J. G. Jacot, P. A. DiMilla, J. Y. Wong, *J. Neural Eng.* **2007**, *4*, 26.